JACS Au
AN OPEN ACCESS JOURNAL OF THE AMERICAN CHEMICAL SOCIETY

pubs.acs.org/jacsau

Perspective

State Interaction Linear Response Time-Dependent Density Functional Theory with Perturbative Spin−Orbit Coupling: Benchmark and Perspectives

Can Liao, Joseph M. Kasper, Andrew J. Jenkins, Ping Yang, Enrique R. Batista, Michael J. Frisch, and Xiaosong Li*

Cite This: *JACS Au* 2023, 3, 358−367

Read Online

ACCESS | Metrics & More | Article Recommendations | Supporting Information

ABSTRACT: Spin−orbit coupling (SOC) is an important driving force in photochemistry. In this work, we develop a perturbative spin−orbit coupling method within the linear response time-dependent density function theory framework (TDDFT-SO). A full state interaction scheme, including singlet−triplet and triplet−triplet coupling, is introduced to describe not only the coupling between the ground and excited states, but also between excited states with all couplings between spin microstates. In addition, expressions to compute spectral oscillator strengths are presented. Scalar relativity is included variationally using the second-order Douglas-Kroll-Hess Hamiltonian, and the TDDFT-SO method is validated against variational SOC relativistic methods for atomic, diatomic, and transition metal complexes to determine the range of applicability and potential limitations. To demonstrate the robustness of TDDFT-SO for large-scale chemical systems, the UV−Vis spectrum of $Au_{25}(SR)_{18}^{-}$ is computed and compared to experiment. Perspectives on the limitation, accuracy, and capability of perturbative TDDFT-SO are presented via analyses of benchmark calculations. Additionally, an open-source Python software package (`PyTDDFT-SO`) is developed and released to interface with the Gaussian 16 quantum chemistry software package to perform this calculation.

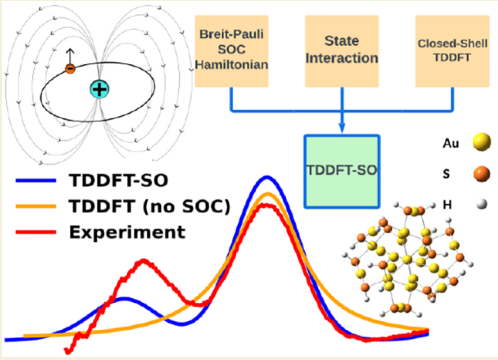

KEYWORDS: *spin−orbit coupling, TDDFT, fine-structure splitting, Breit-Pauli Hamiltonian, transition metal complex*

1. INTRODUCTION

Spin−orbit coupling (SOC) is a cornerstone of modern chemistry, responsible for important photochemical phenomena such as intersystem crossing,[1,2] relativistic spectroscopies (for example, L-edge X-ray absorption,[3] magnetic circular dichroism[4]), and fine-structure splitting.[5] Taking advantage of spin-forbidden processes allowed by SOC has contributed to recent advances throughout chemistry and materials science, especially in LED[6] and solar cell technology.[7,8] With growing popularity in exploring spin-forbidden processes and the ubiquity of nonmain group elements in modern chemistry, there is demand for an efficient SOC method suitable for atomically diverse and large systems.

The time-dependent density functional theory (TDDFT) has been the modern day workhorse for computational photochemistry,[9,10] thanks to the balance between its predictive power and low computational scaling with respect to the system size. There are two types of approaches to include SOC in TDDFT: variational and perturbative. The state-of-the-art variational method that includes SOC in TDDFT employs the Dirac Hamiltonian and a four- or two-component spinor basis.[5,11,12] Two-component approximations to the four-component Dirac Hamiltonian such as the exact two-component (X2C)[5,13−25] Hamiltonian has been successful in reproducing experimental results while staying affordable for small systems.[3,26,27] Although variational relativistic methods are the most complete theoretical treatment of SOC in TDDFT so far, there are challenges that make such an approach less practical for large chemical systems, including the requirements of using complex-valued arithmetic, noncollinear functional forms,[28] and eigensolvers that are effective for a dense manifold of excited states.

In the perturbative approach, the zeroth-order wave function is first variationally determined in the absence of SOC and then SOC is introduced via state interaction to couple states of interest.[29−43] The validity of the perturbative approach depends on the SOC term of the Hamiltonian being much

Received: December 4, 2022
Revised: January 17, 2023
Accepted: January 18, 2023
Published: February 1, 2023

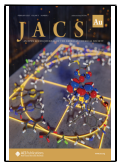

smaller than the excitation energies of the scalar relativistic terms. As high-orders of perturbations are included or as the expansion space increases toward the full CI limit, the perturbative inclusion of SOC should converge to the variational limit. Compared to variational methods, perturbative approaches have some unique advantages, including using one-component real-valued wave functions and hence lower computational cost and less issues with self-consistent-field convergence, as well as identification of spin eigenfunctions in orbital analysis.

State interaction has been successfully adapted for linear response TDDFT through approximate mapping from TDDFT solutions to CIS wave functions,[34,44−48] with a practical Python module developed by Gao et al.[49] However, the limitation and applicability of perturbative spin−orbit approach is not well-known in the community. In this work, we introduce a complete state interaction TDDFT approach to include the SOC effect. The goal is to develop a perturbative TDDFT-SO method that is able to describe couplings between singlet and triplet, as well as between triplet and triplet states for both the ground and excited states. In addition, we explicitly couple spin microstates (for example, $S = 1$, $M_S = -1$, 0, +1) in order to account for anisotropic spin−orbit effects in the full state interaction picture. State-to-state oscillator strengths are also evaluated in the TDDFT-SO framework. The method was implemented in a development version of the Gaussian software package,[50] but is accompanied by an open-source Python module (`PyTDDFT-SO`)[51] that takes Gaussian 16 TDDFT results as input and performs the complete state interaction illustrated in this work.

An extensive benchmark analysis is carried out and compared to variational relativistic X2C-TDDFT results[5] to test the range of applicability of the perturbative TDDFT-SO method. Through this work, we provide the scientific community a practical tool for simulating spin−orbit driven photochemistry and a set of general theoretical guidance on the limitation and applicability of the perturbative spin−orbit approach.

2. METHODOLOGY

2.1. Linear Response Time-Dependent Density Functional Theory

The matrix equation of the linear response time-dependent density functional theory can be written as a non-Hermitian eigenvalue problem:[9,10,52]

$$\begin{pmatrix} \mathbf{A} & \mathbf{B} \\ \mathbf{B}^* & \mathbf{A}^* \end{pmatrix}\begin{pmatrix} \mathbf{X} \\ \mathbf{Y} \end{pmatrix} = \begin{pmatrix} \mathbf{1} & 0 \\ 0 & -\mathbf{1} \end{pmatrix}\begin{pmatrix} \mathbf{X} \\ \mathbf{Y} \end{pmatrix}\begin{pmatrix} \boldsymbol{\omega} & \\ & -\boldsymbol{\omega} \end{pmatrix} \tag{1}$$

$$\boldsymbol{\omega} = \begin{pmatrix} \omega_1 & & \\ & \omega_2 & \\ & & \ddots \end{pmatrix} \tag{2}$$

where ω_I is the excitation energy for the I-th excited state. The I-th column of $\mathbf{X}$ and $\mathbf{Y}$ represent particle-hole and hole-particle excitation amplitudes for the I-th excited state, respectively.[45] The left-most matrix in eq 1, which is related to the orbital Hessian, is given by

$$A_{iajb} = \delta_{ij}\delta_{ab}(E_a - E_i) + (ia|bj) - c_{HF}(ij|ab) + (1 - c_{HF})(ia|V_{XC}|bj) \tag{3}$$

$$B_{iajb} = (ia|jb) - c_{HF}(ib|aj) + (1 - c_{HF})(ia|V_{XC}|jb) \tag{4}$$

where i, j index over occupied orbitals and a, b index over virtual orbitals. The scaling factor c_{HF} modulates the amount of Hartree−Fock exact exchange in the DFT functional ($c_{HF} = 0$ for pure functionals and $c_{HF} \in (0, 1]$ for hybrid functionals).

In the state interaction TDDFT with perturbative spin−orbit, the linear response equation is performed using a restricted Kohn−Sham reference. Because the restricted formalism allows the orbital Hessian to be entirely real-valued, the eigenvalue problem can be reduced to the halved-dimension form:[52]

$$(\mathbf{A} - \mathbf{B})(\mathbf{A} + \mathbf{B})\mathbf{Z} = \mathbf{Z}\boldsymbol{\omega}^2 \tag{5}$$

$$\mathbf{Z} = \mathbf{X} + \mathbf{Y} \tag{6}$$

The excited states are now represented by the columns of $\mathbf{Z}$. The elements of $\mathbf{Z}_I$ represent the contribution of a single orbital excitation toward the I-th excited state. A natural association between these orbital excitations and singly excited Slater determinants can be made. Hence, approximate CIS wave functions can be constructed using $\mathbf{Z}$,[44,45]

$$|I\rangle = \frac{1}{|\mathbf{Z}_I|}\sum_{ia} Z_{ia,I}|\Phi_i^a\rangle \tag{7}$$

2.2. State Interaction with Perturbative Spin−Orbit

In state interaction, an effective Hamiltonian ($\mathbf{H}'$) is constructed by perturbing the zeroth-order Hamiltonian ($\mathbf{H}_0$) with a spin−orbit coupling Hamiltonian ($\mathbf{H}_{SO}$)

$$\mathbf{H}' = \mathbf{H}_0 + \mathbf{H}_{SO} \tag{8}$$

$$[\mathbf{H}_{SO}]_{IJ} = \langle I|\hat{H}_{SO}|J\rangle \tag{9}$$

In the case of LR-TDDFT, the zeroth-order Hamiltonian $\mathbf{H}_0$ is the diagonal matrix of excitation energies with the first diagonal element (ground state) being zero,[34,44]

$$\mathbf{H}_0 = \begin{pmatrix} 0 & \\ & \boldsymbol{\omega} \end{pmatrix} \tag{10}$$

When the spin−orbit coupling is relatively weak compared to the energy difference between spin states, perturbation theory can be used to introduce spin−orbit coupling to a nonrelativistic or spin-free relativistic zeroth-order Hamiltonian. Among the most common spin−orbit operators is the Breit-Pauli spin−orbit operator,[53,54]

$$\hat{H}_{SO} = \frac{1}{2c^2}\left(\sum_{iA}\frac{Z_A}{r_{iA}^3}\hat{\mathbf{l}}_i\cdot\hat{\mathbf{s}}_i - \sum_i\sum_{j\neq i}\frac{1}{r_{ij}^3}\hat{\mathbf{l}}_{ij}\cdot(\hat{\mathbf{s}}_i + 2\hat{\mathbf{s}}_j)\right) \tag{11}$$

where Z_A is the charge of nucleus A, r_{iA} is the distance between electron i and nucleus A, $\hat{\mathbf{l}}_i$ is the orbital angular momentum operator of electron i, and $\hat{\mathbf{s}}_i$ is the spin angular momentum operator. Note that the angular momentum operators can be written in terms of the position and momentum operators so that $\hat{\mathbf{l}}_{ij} = \hat{\mathbf{r}}_{ij} \times \hat{\mathbf{p}}_i$, for example. These terms capture the interactions that give rise to the one-electron (the first term in eq 11) and two-electron spin−orbit couplings (the second term in eq 11). Since the two-electron spin−orbit contribution is computationally expensive to evaluate,[55,56] previous attempts at computing spin−orbit matrix elements approximated two-electron SOC with an effective nuclear charge.[31,46,49,57] However, these effective nuclear charges were only defined for some elements. Here, we use the Boettger factor,[58] which is

https://doi.org/10.1021/jacsau.2c00659
JACS Au 2023, 3, 358−367

available for every element, to approximate two-electron SOC by scaling the one-electron SOC integrals.

The one-electron SOC Hamiltonian can be written in second quantized form shown in eq 12

$$\hat{H}_{\mathrm{SO,1e}} = \sum_{pq}\sum_{\sigma\sigma'} \langle \phi_{p\sigma} | \sum_{A} \frac{Z_A}{2c^2 r_A^3} (\hat{l}_x \hat{s}_x + \hat{l}_y \hat{s}_y + \hat{l}_z \hat{s}_z) | \phi_{q\sigma'} \rangle a_{p\sigma}^{\dagger} a_{q\sigma'} \quad \sigma, \sigma' \in \{\alpha, \beta\} \tag{12}$$

where $\phi_{p\sigma}$, $\phi_{q\sigma'}$ are Kohn−Sham orbitals, and $a_{p\sigma}^{\dagger}$, $a_{q\sigma'}$ are creation and annihilation operators, respectively. In the following equations, we dropped the "1e" notation for brevity. The working expressions can be obtained by partitioning the Hamiltonian into Cartesian components and applying the spin angular momentum operators on $|\phi_{q\sigma'}\rangle$ (see the Supporting Information, SI, for derivations using Wick's theorem),

$$\hat{H}_{\mathrm{SO}} = \hat{H}_{\mathrm{SO}}^{x} + \hat{H}_{\mathrm{SO}}^{y} + \hat{H}_{\mathrm{SO}}^{z} \tag{13}$$

$$\hat{H}_{\mathrm{SO}}^{x} = \frac{1}{2} \sum_{pq} h_{pq}^{x} (a_{p\alpha}^{\dagger} a_{q\beta} + a_{p\beta}^{\dagger} a_{q\alpha}) \tag{14}$$

$$\hat{H}_{\mathrm{SO}}^{y} = -\frac{i}{2} \sum_{pq} h_{pq}^{y} (a_{p\alpha}^{\dagger} a_{q\beta} - a_{p\beta}^{\dagger} a_{q\alpha}) \tag{15}$$

$$\hat{H}_{\mathrm{SO}}^{z} = \frac{1}{2} \sum_{pq} h_{pq}^{z} (a_{p\alpha}^{\dagger} a_{q\alpha} - a_{p\beta}^{\dagger} a_{q\beta}) \tag{16}$$

$$h_{pq}^{k} = \langle \phi_p | \sum_{A} \frac{Z_A}{2c^2 r_A^3} \hat{l}_k | \phi_q \rangle \tag{17}$$

At this point, the Boettger factor is applied to the h_{pq}^{k}. The angular-momentum-dependent factor is applied to the integrals in the atomic orbital (AO) basis,

$$h_{\mu\nu}^{k} = \left(1 - \sqrt{\frac{Q(l_\mu)Q(l_\nu)}{Z_\mu Z_\nu}}\right) h_{\mu\nu}^{k} \tag{18}$$

where l_μ is the orbital angular momentum quantum number of orbital μ, Z_μ is the charge of the nucleus at which orbital μ is centered, and $Q(l)$ is the number of electrons in all filled shell with $n \leq l$. That is, $Q(0) = 0$, $Q(1) = 2$, $Q(2) = 10$, and so forth.

In the restricted Kohn−Sham formalism, electronic states can either be singlets ($S = 0$; $M_S = 0$) or triplets ($S = 1$; $M_S = -1, 0, +1$). When obtaining the analytical expressions for spin−orbit Hamiltonian matrix elements, the states are treated as creation and annihilation operators acting on the Kohn−Sham ground state determinant

$$\text{Singlet, } S = 0, M_S = 0\text{: } |\Phi_i^a\rangle_{0,0} = \frac{1}{\sqrt{2}} (a_{a\alpha}^{\dagger} a_{i\alpha} + a_{a\beta}^{\dagger} a_{i\beta}) |0\rangle \tag{19}$$

$$\text{Triplet, } S = 1, M_S = -1\text{: } |\Phi_i^a\rangle_{1,-1} = a_{a\beta}^{\dagger} a_{i\alpha} |0\rangle \tag{20}$$

$$\text{Triplet, } S = 1, M_S = 0\text{: } |\Phi_i^a\rangle_{1,0} = \frac{1}{\sqrt{2}} (a_{a\alpha}^{\dagger} a_{i\alpha} - a_{a\beta}^{\dagger} a_{i\beta}) |0\rangle \tag{21}$$

$$\text{Triplet, } S = 1, M_S = +1\text{: } |\Phi_i^a\rangle_{1,+1} = -a_{a\alpha}^{\dagger} a_{i\beta} |0\rangle \tag{22}$$

With the electronic states and SOC Hamiltonian clearly defined, expressions for the SOC matrix elements can be derived using Wick's theorem. Here, we only present the final working expression where excited states and their spin quantum numbers are written as $|I_{S,M_S}\rangle$.

The state interaction matrix elements between the closed-shell ground state $|0\rangle$ and excited states are

$$\langle 0 | \hat{H}_{\mathrm{SO}} | J_{1,\pm 1} \rangle = \mp \frac{1}{2|\mathbf{Z}_J|} \sum_{ia} Z_{ia,J} (h_{ia}^{x} \pm i h_{ia}^{y}) \tag{23}$$

$$\langle 0 | \hat{H}_{\mathrm{SO}} | J_{1,0} \rangle = \frac{1}{|\mathbf{Z}_J|\sqrt{2}} \sum_{ia} Z_{ia,J} h_{ia}^{z} \tag{24}$$

$$\langle 0 | \hat{H}_{\mathrm{SO}} | J_{0,0} \rangle = 0 \tag{25}$$

The state interaction matrix elements between excited states are

$$\langle I_{0,0} | \hat{H}_{\mathrm{SO}} | J_{1,\pm 1} \rangle = \frac{1}{2|\mathbf{Z}_I||\mathbf{Z}_J|\sqrt{2}} \left(\sum_{ija} Z_{ia,I} Z_{ja,J} (h_{ji}^{x} \pm i h_{ji}^{y}) - \sum_{iab} Z_{ia,I} Z_{ib,J} (h_{ab}^{x} \pm i h_{ab}^{y}) \right) \tag{26}$$

$$\langle I_{0,0} | \hat{H}_{\mathrm{SO}} | J_{1,0} \rangle = -\frac{1}{2|\mathbf{Z}_I||\mathbf{Z}_J|} \left(\sum_{ija} Z_{ia,I} Z_{ja,J} h_{ji}^{z} + \sum_{iab} Z_{ia,I} Z_{ib,J} h_{ab}^{z} \right) \tag{27}$$

$$\langle I_{1,0} | \hat{H}_{\mathrm{SO}} | J_{1,\pm 1} \rangle = \frac{1}{2|\mathbf{Z}_I||\mathbf{Z}_J|\sqrt{2}} \left(\sum_{ija} Z_{ia,I} Z_{ja,J} (h_{ji}^{x} \pm i h_{ji}^{y}) + \sum_{iab} Z_{ia,I} Z_{ib,J} (h_{ab}^{x} \pm i h_{ab}^{y}) \right) \tag{28}$$

$$\langle I_{1,-1} | \hat{H}_{\mathrm{SO}} | J_{1,1} \rangle = 0 \tag{29}$$

$$\langle I_{1,0} | \hat{H}_{\mathrm{SO}} | J_{1,0} \rangle = 0 \tag{30}$$

$$\langle I_{1,\pm 1} | \hat{H}_{\mathrm{SO}} | J_{1,\pm 1} \rangle = \pm \left(\frac{1}{2} \sum_{ija} Z_{ia,I} Z_{ja,J} h_{ji}^{z} + \frac{1}{2} \sum_{iab} Z_{ia,I} Z_{ib,J} h_{ab}^{z} \right) \tag{31}$$

2.3. Oscillator Strength

After diagonalizing the effective Hamiltonian, we obtain states that include spin−orbit coupling, or spin−orbit adiabatic states,[59] expressed as a linear combination of the unperturbed states,

$$|I\rangle' = \sum_{J} C_{IJ}' |J\rangle \tag{32}$$

where C' is the eigenvector of the effective Hamiltonian. This representation of spin−orbit adiabatic states allows us to obtain transition dipole moments between spin−orbit-coupled

https://doi.org/10.1021/jacsau.2c00659
JACS Au 2023, 3, 358−367

states via transformation of the unperturbed transition dipole moments,

$$\langle 0|\hat{\mathbf{r}}|I'\rangle = \sum_{J} C'_{IJ}\langle 0|\hat{\mathbf{r}}|J\rangle \tag{33}$$

$$\langle I'|\hat{\mathbf{r}}|J'\rangle = \sum_{K,L} C'^{*}_{IK}C'_{JL}\langle K|\hat{\mathbf{r}}|L\rangle \tag{34}$$

Oscillator strengths can be computed using the spin−orbit transition dipole moment (in atomic units) between the ground state and spin−orbit adiabatic excited states

$$f_{0I'} = \frac{2}{3}\omega_{I'}|\langle 0|\hat{\mathbf{r}}|I'\rangle|^2 \tag{35}$$

and between spin−orbit adiabatic excited states,

$$f_{I'J'} = \frac{2}{3}\Delta\omega_{I'J'}|\langle I'|\hat{\mathbf{r}}|J'\rangle|^2 \tag{36}$$

where $\omega_{I'}$ is the eigenvalue of the effective Hamiltonian.

3. BENCHMARK AND DISCUSSION

The state interaction TDDFT-SO method was implemented in the development version of the Gaussian quantum chemistry software package.[50] An open-source code (`PyTDDFT-SO`) that can perform the same algorithm using Gaussian 16[60] as the input is released under the authors GitHub Web site. The zeroth-order Hamiltonian includes the scalar relativity variationally in the ground state DFT calculations via the DKH2 transformation. In this benchmark study, atomic fine structure was compared along with excitation energies of diatomic molecules and transition metal complexes. The UV−Vis spectrum of the Au_{25} nanocluster was also generated by state interaction TDDFT-SO and compared. Benchmark calculations are compared to experiments and the variational X2C-TDDFT approach using the same SOC integrals.[5,26,61]

3.1. Atomic Fine Structure Splitting

In this section, the performance of TDDFT-SO was assessed for atomic cases. Fine structure splitting in the ^{3}P and ^{3}D excited state manifolds were calculated using TDDFT-SO and plotted against variational X2C-TDDFT results. The interaction space chosen for the atomic calculations included the entire manifold of interest, including both singlet and triplet states. Additional states beyond the manifold of interest had negligible effect on the fine structure splitting in the atomic calculations. For the ^{1}S → ^{3}P excitation, two types of electronic transitions are considered here: $s^2 \rightarrow s^1p^1$ and $p^6 \rightarrow p^5s^1$, plotted in Figure 1 and Figure 2. For the ^{1}S → ^{3}D excitation, we plot $s^2 \rightarrow s^1d^1$ and $d^{10} \rightarrow d^9s^1$ transitions in Figure 1 and Figure 2, respectively.

TDDFT-SO is in excellent agreement with X2C-TDDFT for light elements, but tends to overestimate fine structure splitting as the atomic number increases. At $Z > 56$, the number of cases with an unsigned error greater than 0.10 eV drastically increased whereas for $Z \leq 56$, such errors are only seen for highly charged species close to $Z = 56$ (Sb^{3+}, Te^{4+}). This is understandable as the perturbative spin−orbit treatment becomes inadequate when the coupling strength is comparable to the excited state energy gap. Perturbative methods are not expected to hold up at large perturbations. Unlike the ^{3}P manifold, errors for in the ^{3}D manifolds mostly stayed below 0.10 eV up to $Z > 80$. In addition, for the same atom, the error in fine structure splitting increases as the principal quantum number increases.[34] For example, the TDDFT-SO computed Tl^{3+} $^3P_2/^3P_1$ and $^3P_2/^3P_0$ splittings arising from excitation of the 5*p* shell (Figure 2) only have an error of 2% and 11% compared to X2C-TDDFT results. In contrast, when the fine structure splitting is due to the excitation into the 6*p* shell in Tl^+ (Figure 1), the percent error increases to 60% and 84%, respectively. This is likely due to the insufficient number of excited states that is needed to span the spin−orbit operator for outer orbitals.

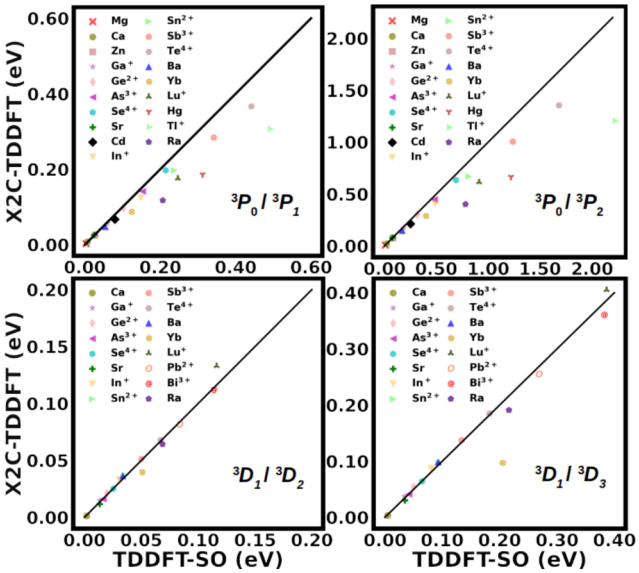

Figure 1. Comparison of excited state fine structure splitting calculated using TDDFT-SO and X2C-TDDFT for various atomic cases. ^{1}S → ^{3}P and ^{1}S → ^{3}D excitations arising from $s^2 \rightarrow s^1p^1$ and $s^2 \rightarrow s^1d^1$ transitions, respectively, are considered. Calculations were done using the ANO-RCC-VTZP basis set[62−66] and the PBE0 functional.[67]

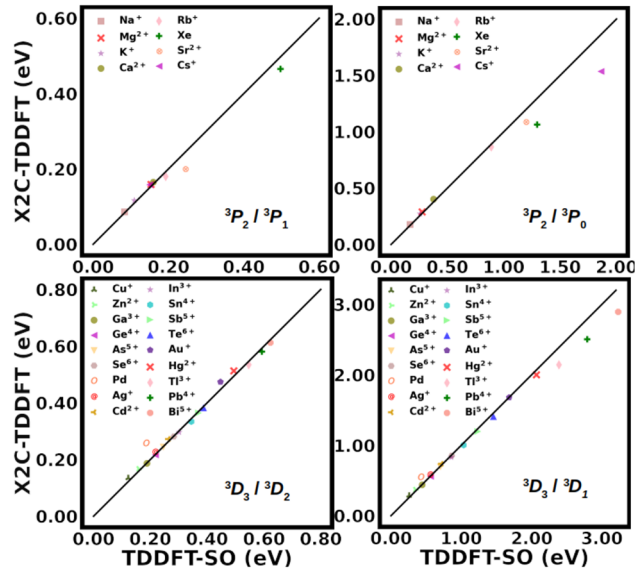

Figure 2. Comparison of excited state fine structure splitting calculated using TDDFT-SO and X2C-TDDFT for various atomic cases. ^{1}S → ^{3}P and ^{1}S → ^{3}D excitations arising from $p^6 \rightarrow p^5s^1$ and $d^{10} \rightarrow d^9s^1$ transitions, respectively, are considered. Calculations were done using the ANO-RCC-VDZ basis set[62−64,66] and the PBE0 functional.[67]

https://doi.org/10.1021/jacsau.2c00659
JACS Au 2023, 3, 358−367

Although the spin−orbit operator does not depend on the choice of DFT functional, the quality of the state interaction TDDFT-SO relies on the quality of the zeroth-order closed-shell TDDFT reference. For example, results for the Yb $^3D_1/^3D_3$ splitting in Figure 1 significantly improved when the BHandH functional[68] was used. Shown in Table 1 are the statistics of TDDFT-SO errors for various functionals. Error is defined as the difference in fine-structure splitting between TDDFT-SO and variational X2C-TDDFT calculations. The computed excitation energies are presented in the SI. For $Z > 56$, starting from the Ln series, all functionals exhibit a significant increase in error, although B3LYP performs slightly better than the other functionals tested, for these heavier elements. This study suggests that perturbative TDDFT-SO is generally reliable for predicting atomic fine structures for elements lighter than the Ln series, but one should be cautious for species with large atomic numbers.

Table 1. Error of TDDFT-SO Atomic Fine Structure Splitting (in eV) Using Different DFT Functionals[a]

	mean AE	max AE	std dev
B3LYP			
$Z \leq 56$	0.0270	0.3627	0.0651
$Z > 56$	0.1798	1.6568	0.3382
BHandH			
$Z \leq 56$	0.0300	0.3306	0.0606
$Z > 56$	0.2724	2.5637	0.5595
PBE			
$Z \leq 56$	0.0284	0.3811	0.0652
$Z > 56$	0.3727	2.4210	0.6526
PBE0			
$Z \leq 56$	0.0289	0.3261	0.0605
$Z > 56$	0.2581	2.4842	0.5171
SVWN			
$Z \leq 56$	0.0266	0.4043	0.0639
$Z > 56$	0.2813	1.6460	0.4281

[a]Absolute error (AE) is defined to be the unsigned error of the TDDFT-SO result compared to X2C-TDDFT.

3.2. Diatomic Molecules

This section assesses the performance of TDDFT-SO on diatomic molecules and the dependence on the size of state interaction space. The equilibrium bond lengths of Cu_2, GaBr, and GaI were obtained from experimental data recorded in the NIST Webbook.[69] Ag_2 and Au_2 bond lengths were optimized using the relativistic CRENBL effective core potential and its corresponding basis set.[66,70,71] All TDDFT calculations were performed using the ANO-RCC-VDZP basis set[63,64,66] and the PBE0 hybrid functional.[67] Five different sizes of state interaction space (N = 5, 10, 15, 20, 50) were used with TDDFT-SO. For a closed-shell ground state, the TDDFT-SO calculation solves for N singlet and N triplet states, resulting in an interaction space of $4N + 1$ states, including the ground state and each triplet microstate.

Table 2 tabulates the statistics of TDDFT-SO errors for excited state energy calculations of diatomic molecules. Error is defined as the difference in calculated excitation energy between TDDFT-SO and variational X2C-TDDFT. The computed excitation energies are presented in the SI. Table 2 shows that TDDFT-SO results are in good agreement with X2C-TDDFT even with the smallest interaction space N = 5.

Table 2. Error of TDDFT-SO Excitation Energies (in eV) of Diatomic Molecules Using Various Interaction Spaces[a]

	interaction space				
	N = 5	N = 10	N = 15	N = 20	N = 50
Cu_2					
mean AE	0.0282	0.0048	0.0048	0.0047	0.0047
max AE	0.1411	0.0106	0.0106	0.0107	0.0108
std dev	0.0441	0.0035	0.0037	0.0037	0.0038
Ag_2					
mean AE	0.0195	0.0137	0.0105	0.0113	0.0120
max AE	0.0536	0.0536	0.0195	0.0202	0.0218
std dev	0.0184	0.0160	0.0070	0.0072	0.0075
Au_2					
mean AE	0.1280	0.1098	0.1339	0.1464	0.1586
max AE	0.5142	0.1510	0.1644	0.1814	0.1957
std dev	0.1510	0.0473	0.0266	0.0269	0.0330
GaBr					
mean AE	0.0114	0.0058	0.0062	0.0064	0.0069
max AE	0.0904	0.0200	0.0225	0.0225	0.0233
std dev	0.0297	0.0072	0.0077	0.0077	0.0079
GaI					
mean AE	0.0464	0.0384	0.0392	0.0396	0.0419
max AE	0.2248	0.0702	0.0705	0.0707	0.0746
std dev	0.0708	0.0221	0.0223	0.0224	0.0229

[a]Absolute error (AE) is defined to be the unsigned error of the TDDFT-SO result compared to X2C-TDDFT.

The agreement deteriorates with increasing Z. For Au_2 (Z = 79) with N = 5, we observed a mean-average-error of ∼0.1 eV. Errors in TDDFT-SO calculated excitation energies can be improved with a larger interaction space. As the interaction space increases, the spin−orbit operator is more accurately represented in the expansion of zeroth-order eigenstates. In the limit of infinite order response theory (equivalent to the full CI limit), it should converge to the exact solution. Table 2 shows that as the interaction space increases, the standard deviation of TDDFT-SO errors decreases. With N = 50 (201 states), TDDFT-SO errors are only at the meV level for most diatomic molecules studied here.

Readers should note that all microstates (S = 1, M_S = −1, 0, +1) that belong to a same triplet manifold must be included in the interaction space. Failing to do so will cause unphysical degeneracy and Kramers' symmetry breaking.

3.3. Transition Metal Complexes

In this section, we further assess the performance of TDDFT-SO by applying the method to transition metal complexes. High symmetry complexes, consisting of late-row transition metals (Mo, W, Pd, Ru, and Os), were chosen to showcase the interplay between spin−orbit coupling and the ligand field. All geometries were optimized using the PBE0 hybrid functional[67] with the CRENBL effective core potential[66,70,71] and its corresponding basis set. The TDDFT calculations were performed using the PBE0 hybrid functional with the relativistically optimized double-ζ Sapporo-2012 basis set including diffuse functions[66,72,73] for metal centers and the nonrelativistic Pople 6-311G(d,p) basis sets[66,74−76] for ligands.

The computed excitation energies of the lowest several excited states for each transition metal complex are presented in the SI. Table 3 shows the statistics of errors defined as the difference in excitation energy between TDDFT-SO and X2C-TDDFT. The results are consistent with those obtained for

https://doi.org/10.1021/jacsau.2c00659
JACS Au 2023, 3, 358−367

Table 3. Error of TDDFT-SO Excitation Energies (in eV) of Transition Metal Complexes Using Various Interaction Spaces[a]

	interaction space				
	$N = 6$	$N = 10$	$N = 15$	$N = 20$	$N = 60$
$Mo(CO)_6$					
mean AE	0.0099	0.0027	0.0027	0.0027	0.0027
max AE	0.0368	0.0068	0.0070	0.0070	0.0070
std dev	0.0120	0.0021	0.0022	0.0022	0.0022
$W(CO)_6$					
mean AE	0.0101	0.0171	0.0182	0.0187	0.0188
max AE	0.0399	0.0293	0.0299	0.0299	0.0300
std dev	0.0130	0.0070	0.0074	0.0071	0.0071
$PdCl_6^{2-}$					
mean AE	0.0042	0.0031	0.0014	0.0013	0.0023
max AE	0.0074	0.0052	0.0031	0.0032	0.0055
std dev	0.0023	0.0017	0.0011	0.0011	0.0016
RuO_4					
mean AE	0.0087	0.0086	0.0084	0.0077	0.0078
max AE	0.0163	0.0159	0.0150	0.0130	0.0130
std dev	0.0064	0.0063	0.0056	0.0054	0.0045
OsO_4					
mean AE	0.0692	0.0665	0.0540	0.0425	0.0286
max AE	0.0968	0.0948	0.0885	0.0649	0.0600
std dev	0.0234	0.0239	0.0262	0.0218	0.0232

[a]Absolute error (AE) is defined to be the unsigned error of the TDDFT-SO result compared to X2C-TDDFT.

atomic and diatomic species with the sixth-row elements, W ($Z = 74$) and Os ($Z = 76$), exhibiting relatively large yet acceptable errors (less than 0.1 eV) compared to the variational X2C-TDDFT calculations.

The TDDFT-SO errors shown in transition metal complexes are smaller than those for diatomic molecules. In transition metal complexes with light-element ligands, the metal center is the main contributor of the spin−orbit coupling. In contrast, the diatomic molecules presented in Table 2 include *two* elements having significant spin−orbit characters, resulting in many strongly coupled states. As a result, for a similar size of interaction space, TDDFT-SO has a smaller error for transition metal complexes with a single main spin−orbit center than diatomic molecules with two spin−orbit centers.

3.4. UV−Vis Spectrum of $Au_{25}(SH)_{18}^-$

As a low-scaling method, the state interaction TDDFT-SO method is uniquely suited for studying large scale systems, such as metal nanoclusters. Figure 3 compares perturbative TDDFT-SO spectrum of a Au_{25} cluster with variational two-component TDDFT (2c-TDDFT) where scalar relativity and spin−orbit coupling were captured through the CRENBL effective core potential.[70,71,77−79] The nonrelativistic TDDFT (no SOC term) spectrum is also included for comparison. All electrons were treated explicitly in the TDDFT-SO calculation using the DKH-optimized triple-ζ Jorge basis set with polarization functions for the Au atoms[66,80] and the non-relativistic Pople 6-31G(d,p)[66,75,81] and 6-31G basis sets[66,82] for S and H atoms, respectively. The PBE0 hybrid functional[67] was used in both the TDDFT-SO and two-component TDDFT calculations. Although the experimental spectrum[83] was obtained using $Au_{25}(SPET)_{18}^-$, whereas the computed spectra used the model system $Au_{25}(SH)_{18}^-$, it is known in the literature that the choice of ligands minimally affects the fingerprint band.[84]

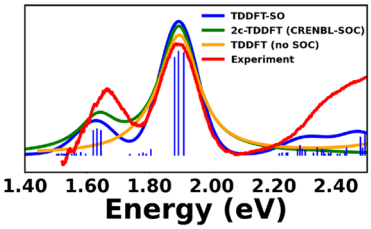

Figure 3. UV−Vis spectrum of $Au_{25}(SR)_{18}^-$. Computed spectra are shifted, broadened, and normalized to align with the large peak at 1.90 eV. Excited states from TDDFT-SO are indicated by blue sticks, where the height is scaled by the oscillator strength. The full-width half-max was set to 0.07 eV. Experimental spectrum reproduced from ref 83. Copyright 2011 American Chemical Society.

Because they possess a large number of degrees of freedom, Jahn−Teller distortion causes most nanoclusters with an even number of electrons to have a closed-shell ground state.[85] A study by Jiang et al. showed that spin−orbit coupling plays a large role in $Au_{25}(SR)_{18}^-$ nanocluster valence excitations.[86]Fig-Figure 3 shows that the splitting of the "fingerprint" absorption band at 1.60−2.00 eV was due to spin−orbit coupling. This splitting is clearly absent in the nonrelativistic TDDFT calculation. The TDDFT-SO spectrum compared remarkably, in both relative peak position and intensity, to results from experiment and 2c-TDDFT.

3.5. Partial Failure of State Interaction TDDFT-SO

As in all perturbative spin−orbit coupling treatment, when the spin−orbit strength is comparable in magnitude to ligand field or other electron−electron repulsion effects, the state interaction picture becomes inadequate. This failure is particularly acute when the interaction space is small and when the excitation is only limited to the first order. Figure 4 shows the molecular orbital and state energy diagrams of $PtCl_6^{2-}$. The energy difference between the spin-free t_{2g} (Pt-*d*) and t_{1g} (Cl-*p*) orbitals in this case is computed to be ∼0.09 eV. The spin−orbit coupling (∼0.39 eV) for the t_{2g} manifold splits the t_{2g} manifold into two groups with two levels higher in energy than t_{1g}. Electronic excitations from the occupied orbitals to the unoccupied space in TDDFT gives rise to the state energy diagram (right side of Figure 4) which is labeled with double group notations. These are energy ordering expected from a variational X2C-TDDFT calculation.

Table 4 shows the TDDFT-SO computed ordering of excited states in $PtCl_6^{2-}$ compared to variational X2C-TDDFT results. It is evident that the TDDFT-SO incorrectly predicted the ordering of excited states. It is understandable that TDDFT-SO will have difficulty in resolving small (<20 meV) energy difference (for example, A_{2g} vs $^3T_{2g}$) given the statistics of errors presented in the previous section. However, we also observed an incorrect ordering for states with a large gap (A_{1g} vs E_g in Table 4) This error, however, cannot be reconciled by simply increasing the interaction space. Accurately capturing spin−orbit coupling in TDDFT-SO may require constructing the effective Hamiltonian in an interaction space closer to the infinite-order response theory limit since linear response TDDFT can only provide a full CIS equivalent interaction space. Strong spin−orbit coupling will still require excitation operators beyond singles.

https://doi.org/10.1021/jacsau.2c00659
JACS Au 2023, 3, 358−367

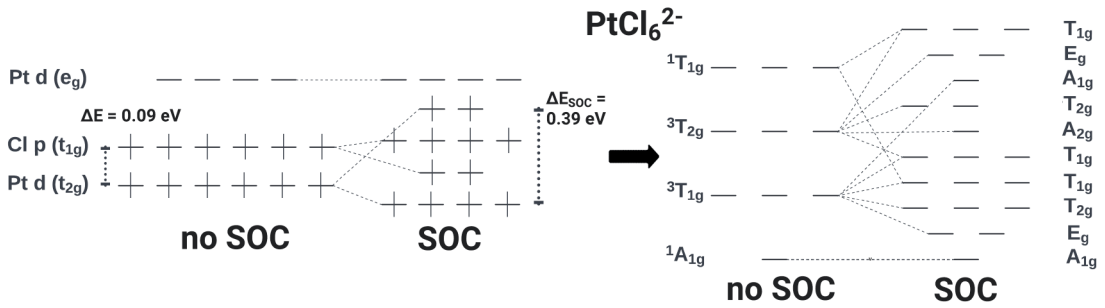

Figure 4. Left: Molecular orbital (MO) diagram of $PtCl_6^{2-}$. Each level is a single spin−orbital, with electrons represented by vertical bars. The MO diagram without SOC was obtained from the restricted Kohn−Sham reference used in TDDFT-SO. The MO diagram with SOC was obtained from the X2C Kohn−Sham reference used in X2C-TDDFT. Right: State diagram of $PtCl_6^{2-}$. Each state is described by its irreducible representation in $G \times SU(2)$, where G is the spatial symmetry group of the molecule.

Table 4. Comparison between Excitation Energies of $PtCl_6^{2-}$ Calculated Using X2C-TDDFT and TDDFT-SO with an Interaction Space of N Singlet and N Triplet Spin-Free States[a]

state	TDDFT-SO					X2C-TDDFT
	$N = 6$	$N = 10$	$N = 15$	$N = 20$	$N = 60$	
E_g	1.8010	1.7851	1.7835	1.7835	1.7624	1.8648
T_{2g}	1.8697	1.8584	1.8573	1.8574	1.8334	1.9492
T_{1g}	1.9167	1.9015	1.9006	1.9006	1.8780	1.9691
T_{1g}	2.3104	2.3096	2.3082	2.3082	2.2640	2.3607
A_{2g}	2.3867	2.3542	2.3590	2.3590	2.3358	2.3646
T_{2g}	2.3727	2.3565	2.3572	2.3573	2.3261	2.4046
A_{1g}	**2.5220**	**2.5131**	**2.4966**	**2.4966**	**2.4630**	2.4051
E_g	**2.3552**	**2.3578**	**2.3513**	**2.3513**	**2.3180**	2.4121
T_{1g}	2.5832	2.5630	2.5627	2.5627	2.5232	2.5824

[a]Each state is described by its irreducible representation in $G \times SU(2)$, where G is the spatial symmetry group of the molecule. States with large singlet-triplet mixing is written as a direct sum of the singlet and triplet irreducible representations. Notation was adopted from Altmann and Herzig.[87] The ordering of highlighted states are incorrectly predicted by TDDFT-SO with a >0.1 eV error.

4. CONCLUSIONS AND PERSPECTIVE

TDDFT-SO, a perturbative SOC method for TDDFT, was developed within the state interaction framework. Scalar relativity was included variationally in the restricted Kohn−Sham reference. The TDDFT excited states are used as the zeroth-order wave function with one-electron spin−orbit operator in the TDDFT-SO formalism. Analytical expressions are presented to compute the spin−orbit coupled Hamiltonian matrix with zeroth-order wave function being spin microstates from a linear response TDDFT calculation. Two-electron SOC was approximated using the Boettger factor. Expressions to compute oscillator strengths between spin−orbit adiabatic states are also presented. In addition to the implementation in the development version of the Gaussian software package, an open-source Python code (`PyTDDFT-SO`) was developed to interface with Gaussian 16 to perform this method.

TDDFT-SO was tested against X2C-TDDFT for atoms, diatomic molecules, and transition metal complexes. TDDFT-SO results for atomic fine structure splitting agreed very well overall with X2C-TDDFT for light elements, but the performance deteriorates toward late-row elements as expected. Studies of diatomic molecules and transition metal complexes show that the accuracy of the TDDFT-SO approach can be improved by increasing the size of the interaction space.

The motivation for this work was to increase the accessibility of SOC methods in TDDFT for large systems. TDDFT-SO was able to produce the UV−Vis spectrum of the $Au_{25}(SR)_{18}^{-}$ nanocluster. The spectrum generated by TDDFT-SO is nearly identical to the X2C-TDDFT result and is in good agreement with experiment. While the method is widely applicable to most spin−orbit-driven chemical processes in light elements, the benchmark case of $PtCl_6^{2-}$ exemplifies the limitation of the state interaction TDDFT-SO when the spin−orbit strength is stronger than the energy splitting as TDDFT-SO incorrectly predicted the ordering of excited states. Caution must be taken when applying the TDDFT-SO approach to late-row elements:

- Perturbative TDDFT-SO generally performs well for light element $Z \leq 56$. Starting from the Ln series, TDDFT-SO error increases significantly, although increasing the interaction space size can aid reducing the error.
- Readers should note that all microstates ($S = 1$, $M_S = -1, 0, +1$) that belong to a same triplet manifold must be included in the interaction space. Failing to do so will cause degeneracy and Kramers' symmetry breaking.
- When the molecular system include multiple spin−orbit centers, a large interaction space is needed to produce satisfactory result using TDDFT-SO.
- The TDDFT-SO approach requires a closed-shell ground state reference. This is because the analytical expressions for perturbative spin−orbit operators are defined in the spin eigenspace. When the ground state is of an open-shell character, variational relativistic TDDFT methods[5,26,61,88] should be used.

The TDDFT-SO approach developed here also works with interior spin-free states using the energy-specific algorithm.[89−91] In principle, the algorithm also works with effective-core-potentials (ECP), provided that the ECP is parametrized and calibrated for use with perturbative spin−orbit coupling, which requires an accurate description of the valence orbitals close to the nucleus. These important topics will be future investigations.

■ ASSOCIATED CONTENT

Supporting Information

The Supporting Information is available free of charge at https://pubs.acs.org/doi/10.1021/jacsau.2c00659.

https://doi.org/10.1021/jacsau.2c00659
JACS Au 2023, 3, 358−367

Derivations of SOC matrix element using Wick's theorem, atomic fine-structure splitting computed with different DFT functionals, excitation energies of diatomic molecules, and excitation energies of transition metal complexes (PDF)

Input geometries for all molecular species (TXT)

AUTHOR INFORMATION

Corresponding Author

Xiaosong Li − *Department of Chemistry, University of Washington, Seattle, Washington 98195, United States;* orcid.org/0000-0001-7341-6240; Email: xsli@uw.edu

Authors

Can Liao − *Department of Chemistry, University of Washington, Seattle, Washington 98195, United States*

Joseph M. Kasper − *Theoretical Division, Los Alamos National Laboratory, Los Alamos, New Mexico 87545, United States;* orcid.org/0000-0002-3840-484X

Andrew J. Jenkins − *Department of Chemistry, University of Washington, Seattle, Washington 98195, United States;* orcid.org/0000-0002-1014-5225

Ping Yang − *Theoretical Division, Los Alamos National Laboratory, Los Alamos, New Mexico 87545, United States;* orcid.org/0000-0003-4726-2860

Enrique R. Batista − *Theoretical Division, Los Alamos National Laboratory, Los Alamos, New Mexico 87545, United States;* orcid.org/0000-0002-3074-4022

Michael J. Frisch − *Gaussian Inc., Wallingford, Connecticut 06492, United States*

Complete contact information is available at: https://pubs.acs.org/10.1021/jacsau.2c00659

Author Contributions

CRediT: **Can Liao** data curation, investigation, methodology, software, validation, writing-original draft; **Joseph M. Kasper** conceptualization, resources, writing-original draft, writing-review & editing; **Andrew J. Jenkins** methodology, software, supervision, writing-review & editing; **Ping Yang** funding acquisition, investigation, project administration, writing-review & editing; **Enrique R. Batista** funding acquisition, investigation, project administration, resources, writing-review & editing; **Michael J. Frisch** software, writing-review & editing; **Xiaosong Li** conceptualization, data curation, formal analysis, funding acquisition, investigation, methodology, project administration, resources, software, supervision, validation, writing-original draft, writing-review & editing.

Notes

The authors declare no competing financial interest.

ACKNOWLEDGMENTS

The development of state interaction spin−orbit methods for computing excited state couplings is supported by the Air Force Office of Scientific Research (grant no. FA9550-21-1-0344). Computations were facilitated through the use of advanced computational, storage, and networking infrastructure provided by the Hyak supercomputer system at the University of Washington, funded by the Student Technology Fee. Part of this work was conducted at Los Alamos National Laboratory, which is operated for the National Nuclear Security Administration of DOE by Triad National Security, LLC (Contract 89233218CNA000001). E.R.B. and P.Y. gratefully acknowledge the U.S. Department of Energy, Office of Science (DOE OS), Basic Energy Sciences (BES) Heavy Element Chemistry Program (HEC) at LANL (Contract DE-AC52-06NA25396). C.L. acknowledges support from the Seaborg Institute at LANL. J.M.K. gratefully acknowledges support from a Director's Postdoctoral Fellowship at LANL.

REFERENCES

(1) Marian, C. M. Spin-Orbit Coupling and Intersystem Crossing in Molecules. *WIREs Comput. Mol. Sci.* **2012**, *2*, 187−203.

(2) Valentine, A. J. S.; Li, X. Intersystem Crossings in Late-Row Elements: A Perspective. *J. Phys. Chem. Lett.* **2022**, *13*, 3039−3046.

(3) Kasper, J. M.; Stetina, T. F.; Jenkins, A. J.; Li, X. Ab Initio Methods for L-Edge X-Ray Absorption Spectroscopy. *Chem. Phys. Rev.* **2020**, *1*, 011304.

(4) Sun, S.; Li, X. Relativistic Effects in Magnetic Circular Dichroism: Restricted Magnetic Balance and Temperature Dependence. *J. Chem. Theory Comput.* **2020**, *16*, 4533−4542.

(5) Egidi, F.; Sun, S.; Goings, J. J.; Scalmani, G.; Frisch, M. J.; Li, X. Two-Component Non-Collinear Time-Dependent Spin Density Functional Theory for Excited State Calculations. *J. Chem. Theory Comput.* **2017**, *13*, 2591−2603.

(6) Uoyama, H.; Goushi, K.; Shizu, K.; Nomura, H.; Adachi, C. Highly Efficient Organic Light-Emitting Diodes from Delayed Fluorescence. *Nature* **2012**, *492*, 234−238.

(7) Wu, W.; Guo, H.; Wu, W.; Ji, S.; Zhao, J. Organic Triplet Sensitizer Library Derived from a Single Chromophore (BODIPY) with Long-Lived Triplet Excited State for Triplet-Triplet Annihilation Based Upconversion. *J. Org. Chem.* **2011**, *76*, 7056−7064.

(8) Pristash, S. R.; Corp, K. L.; Rabe, E. J.; Schlenker, C. W. Heavy-Atom-Free Red-to-Yellow Photon Upconversion in a Thiosquaraine Composite. *ACS Appl. Energy Mater.* **2020**, *3*, 19−28.

(9) Casida, M. E. In *Recent Advances in Density Functional Methods (Part I)*; Chong, D., Ed.; World Scientific: Singapore, 1995; p 155.

(10) Dreuw, A.; Head-Gordon, M. Single-Reference ab Initio Methods for the Calculation of Excited States of Large Molecules. *Chem. Rev.* **2006**, *37*, 832−839.

(11) Gao, J.; Liu, W.; Song, B.; Liu, C. Time-Dependent Four-Component Relativistic Density Functional Theory for Excitation Energies. *J. Chem. Phys.* **2004**, *121*, 6658−6666.

(12) Gao, J.; Zou, W.; Liu, W.; Xiao, Y.; Peng, D.; Song, B.; Liu, C. Time-Dependent Four-Component Relativistic Density-Functional Theory for Excitation Energies. II. The Exchange-Correlation Kernel. *J. Chem. Phys.* **2005**, *123*, 054102.

(13) Kutzelnigg, W.; Liu, W. Quasirelativistic Theory Equivalent to Fully Relativistic Theory. *J. Chem. Phys.* **2005**, *123*, 241102.

(14) Liu, W.; Peng, D. Infinite-Order Quasirelativistic Density Functional Method Based on the Exact Matrix Quasirelativistic Theory. *J. Chem. Phys.* **2006**, *125*, 044102.

(15) Peng, D.; Liu, W.; Xiao, Y.; Cheng, L. Making Four- and Two-Component Relativistic Density Functional Methods Fully Equivalent Based on the Idea of From Atoms to Molecule. *J. Chem. Phys.* **2007**, *127*, 104106.

(16) Ilias, M.; Saue, T. An Infinite-Order Relativistic Hamiltonian by a Simple One-Step Transformation. *J. Chem. Phys.* **2007**, *126*, 064102.

(17) Liu, W.; Peng, D. Exact Two-component Hamiltonians Revisited. *J. Chem. Phys.* **2009**, *131*, 031104.

(18) Liu, W. Ideas of Relativistic Quantum Chemistry. *Mol. Phys.* **2010**, *108*, 1679−1706.

(19) Saue, T. Relativistic Hamiltonians for Chemistry: A Primer. *ChemPhysChem* **2011**, *12*, 3077−3094.

(20) Li, Z.; Xiao, Y.; Liu, W. On the Spin Separation of Algebraic Two-Component Relativistic Hamiltonians. *J. Chem. Phys.* **2012**, *137*, 154114.

(21) Peng, D.; Middendorf, N.; Weigend, F.; Reiher, M. An Efficient Implementation of Two-Component Relativistic Exact-Decoupling Methods for Large Molecules. *J. Chem. Phys.* **2013**, *138*, 184105.

(22) Egidi, F.; Goings, J. J.; Frisch, M. J.; Li, X. Direct Atomic-Orbital-Based Relativistic Two-Component Linear Response Method for Calculating Excited-State Fine Structures. *J. Chem. Theory Comput.* **2016**, *12*, 3711−3718.
(23) Goings, J. J.; Kasper, J. M.; Egidi, F.; Sun, S.; Li, X. Real Time Propagation of the Exact Two Component Time-Dependent Density Functional Theory. *J. Chem. Phys.* **2016**, *145*, 104107.
(24) Konecny, L.; Kadek, M.; Komorovsky, S.; Malkina, O. L.; Ruud, K.; Repisky, M. Acceleration of Relativistic Electron Dynamics by Means of X2C Transformation: Application to the Calculation of Nonlinear Optical Properties. *J. Chem. Theory Comput.* **2016**, *12*, 5823−5833.
(25) Liu, J.; Cheng, L. Relativistic Coupled-Cluster and Equation-of-Motion Coupled-Cluster Methods. *WIREs Comput. Mol. Sci.* **2021**, *11*, 1536.
(26) Stetina, T. F.; Kasper, J. M.; Li, X. Modeling $L_{2,3}$-Edge X-ray Absorption Spectroscopy with Linear Response Exact Two-Component Relativistic Time-Dependent Density Functional Theory. *J. Chem. Phys.* **2019**, *150*, 234103.
(27) Kasper, J. M.; Li, X. Natural Transition Orbitals for Complex Two-Component Excited State Calculations. *J. Comput. Chem.* **2020**, *41*, 1557−1563.
(28) Goings, J. J.; Egidi, F.; Li, X. Current Development of Non-collinear Electronic Structure Theory. *Int. J. Quantum Chem.* **2018**, *118*, e25398.
(29) Heß, B. A.; Marian, C. M.; Wahlgren, U.; Gropen, O. A Mean-field Spin-orbit Method Applicable to Correlated Wavefunctions. *Chem. Phys. Lett.* **1996**, *251*, 365−371.
(30) Berning, A.; Schweizer, M.; Werner, H.-J.; Knowles, P. J.; Palmieri, P. Spin-Orbit Matrix Elements for Internally Contracted Multireference Configuration Interaction Wavefunctions. *Mol. Phys.* **2000**, *98*, 1823−1833.
(31) Koseki, S.; Fedorov, D. G.; Schmidt, M. W.; Gordon, M. S. Spin-Orbit Splittings in the Third-Row Transition Elements: Comparison of Effective Nuclear Charge and Full Breit-Pauli Calculations. *J. Phys. Chem. A* **2001**, *105*, 8262−8268.
(32) Malmqvist, P. A.; Roos, B.; Schimmelpfennig, B. The Restricted Active Space (RAS) State Interaction Approach with Spin−Orbit Coupling. *Chem. Phys. Lett.* **2002**, *357*, 230−240.
(33) Roos, B.; Malmqvist, P. A. Relativistic Quantum Chemistry: The Multiconfigurational Approach. *Phys. Chem. Chem. Phys.* **2004**, *6*, 2919−2927.
(34) Wang, F.; Ziegler, T. A Simplified Relativistic Time-Dependent Density-Functional Theory Formalism for the Calculations of Excitation Energies Including Spin-Orbit Coupling Effect. *J. Chem. Phys.* **2005**, *123*, 154102.
(35) Wang, F.; Gauss, J.; van Wüllen, C. Closed-shell Coupled-cluster Theory with Spin-orbit Coupling. *J. Chem. Phys.* **2008**, *129*, 064113.
(36) Wang, Z.; Wang, F. Spin-Orbit Coupling and Electron Correlation at Various Coupled-cluster Levels for Closed-shell Diatomic Molecules. *Phys. Chem. Chem. Phys.* **2013**, *15*, 17922−17928.
(37) Epifanovsky, E.; Klein, K.; Stopkowicz, S.; Gauss, J.; Krylov, A. Spin-Orbit Couplings within the Equation-of-Motion Coupled-Cluster Framework: Theory, Implementation, and Benchmark Calculations. *J. Chem. Phys.* **2015**, *143*, 064102.
(38) Cheng, L.; Wang, F.; Stanton, J. F.; Gauss, J. Perturbative Treatment of Spin-orbit-coupling within Spin-free Exact Two-component Theory using Equation-of-motion Coupled-cluster Methods. *J. Chem. Phys.* **2018**, *148*, 044108.
(39) Mussard, B.; Sharma, S. One-Step Treatment of Spin−Orbit Coupling and Electron Correlation in Large Active Spaces. *J. Chem. Theory Comput.* **2018**, *14*, 154−165.
(40) Bokhan, D.; Trubnikov, D. N.; Perera, A.; Bartlett, R. J. Spin-orbit Split Ionized and Electron-attached States using Explicitly-Correlated Equation-of-motion Coupled-cluster Singles and Doubles Eigenvectors. *Chem. Phys. Lett.* **2019**, *730*, 372−377.
(41) Vidal, M. L.; Pokhilko, P.; Krylov, A. I.; Coriani, S. Equation-of-Motion Coupled-Cluster Theory to Model L-Edge X-ray Absorption and Photoelectron Spectra. *J. Phys. Chem. Lett.* **2020**, *11*, 8314−8321.
(42) Meitei, O. R.; Houck, S. E.; Mayhall, N. J. Spin−Orbit Matrix Elements for a Combined Spin-Flip and IP/EA Approach. *J. Chem. Theory Comput.* **2020**, *16*, 3597−3606.
(43) Carreras, A.; Jiang, H.; Pokhilko, P.; Krylov, A. I.; Zimmerman, P. M.; Casanova, D. Calculation of Spin−orbit Couplings using RASCI Spinless One-particle Density Matrices: Theory and Applications. *J. Chem. Phys.* **2020**, *153*, 214107.
(44) Li, Z.; Suo, B.; Zhang, Y.; Xiao, Y.; Liu, W. Combining Spin-Adapted Open-Shell TD-DFT with Spin−Orbit Coupling. *Mol. Phys.* **2013**, *111*, 3741−3755.
(45) Franco de Carvalho, F.; Curchod, B. F. E.; Penfold, T. J.; Tavernelli, I. Derivation of Spin-Orbit Couplings in Collinear Linear-Response TDDFT: A Rigorous Formulation. *J. Chem. Phys.* **2014**, *140*, 144103.
(46) de Souza, B.; Farias, G.; Neese, F.; Izsák, R. Predicting Phosphorescence Rates of Light Organic Molecules Using Time-Dependent Density Functional Theory and the Path Integral Approach to Dynamics. *J. Chem. Theory Comput.* **2019**, *15*, 1896−1904.
(47) Bellonzi, N.; Alguire, E.; Fatehi, S.; Shao, Y.; Subotnik, J. E. TD-DFT Spin-adiabats with Analytic Nonadiabatic Derivative Couplings. *J. Chem. Phys.* **2020**, *152*, 044112.
(48) Kotaru, S.; Pokhilko, P.; Krylov, A. I. Spin−Orbit Couplings within Spin-Conserving and Spin-Flipping Time-Dependent Density Functional Theory: Implementation and Benchmark Calculations. *J. Chem. Phys.* **2022**, *157*, 224110.
(49) Gao, X.; Bai, S.; Fazzi, D.; Niehaus, T.; Barbatti, M.; Thiel, W. Evaluation of Spin-Orbit Couplings with Linear-Response Time-Dependent Density Functional Methods. *J. Chem. Theory Comput.* **2017**, *13*, 515−524.
(50) Frisch, M. J.; Trucks, G. W.; Schlegel, H. B.; Scuseria, G. E.; Robb, M. A.; Cheeseman, J. R.; Scalmani, G.; Barone, V.; Petersson, G. A.; Nakatsuji, H.; Li, X.; Caricato, M.; Marenich, A. V.; Bloino, J.; Janesko, B. G.; Gomperts, R.; Mennucci, B.; Hratchian, H. P.; Ortiz, J. V.; Izmaylov, A. F.; Sonnenberg, J. L.; Williams-Young, D.; Ding, F.; Lipparini, F.; Egidi, F.; Goings, J.; Peng, B.; Petrone, A.; Henderson, T.; Ranasinghe, D.; Zakrzewski, V. G.; Gao, J.; Rega, N.; Zheng, G.; Liang, W.; Hada, M.; Ehara, M.; Toyota, K.; Fukuda, R.; Hasegawa, J.; Ishida, M.; Nakajima, T.; Honda, Y.; Kitao, O.; Nakai, H.; Vreven, T.; Throssell, K.; Montgomery, J. A., Jr.; Peralta, J. E.; Ogliaro, F.; Bearpark, M. J.; Heyd, J. J.; Brothers, E. N.; Kudin, K. N.; Staroverov, V. N.; Keith, T. A.; Kobayashi, R.; Normand, J.; Raghavachari, K.; Rendell, A. P.; Burant, J. C.; Iyengar, S. S.; Tomasi, J.; Cossi, M.; Millam, J. M.; Klene, M.; Adamo, C.; Cammi, R.; Ochterski, J. W.; Martin, R. L.; Morokuma, K.; Farkas, O.; Foresman, J. B.; Fox, D. J.Gaussian Development Version Revision J.14+.
(51) Liao, C.; Li, X.PyTDDFT-SO. https://github.com/xsligroup/PyTDDFT-SO (accessed 2022−11−17, git hash 282ba6c04ec18-f104ed4983fe14137eee93c9cc8), 2022.
(52) Stratmann, R. E.; Scuseria, G. E.; Frisch, M. J. An Efficient Implementation of Time-Dependent Density-Functional Theory for the Calculation of Excitation Energies of Large Molecules. *J. Chem. Phys.* **1998**, *109*, 8218−8224.
(53) Dyall, K. G.; Faegri, K.*Introduction to Relativistic Quantum Chemistry*; Oxford University Press, Inc.: Oxford, U.K., 2007.
(54) Reiher, M.; Wolf, A.*Relativistic Quantum Chemistry*, 2nd ed.; Wiley-VCH: Weinheim, 2015.
(55) Sun, S.; Stetina, T. F.; Zhang, T.; Hu, H.; Valeev, E. F.; Sun, Q.; Li, X. Efficient Four-Component Dirac−Coulomb−Gaunt Hartree−Fock in the Pauli Spinor Representation. *J. Chem. Theory Comput.* **2021**, *17*, 3388−3402.
(56) Sun, S.; Ehrman, J. N.; Sun, Q.; Li, X. Efficient Evaluation of the Breit Operator in the Pauli Spinor Basis. *J. Chem. Phys.* **2022**, *157*, 064112.

(57) Chiodo, S. G.; Russo, N. One-Electron Spin-Orbit Contribution by Effective Nuclear Charges. *J. Comput. Chem.* **2009**, *30*, 832−839.
(58) Boettger, J. C. Approximate Two-Electron Spin-Orbit Coupling Term for Density-Functional-Theory DFT Calculations Using the Douglas-Kroll-Hess Transformation. *Phys. Rev. B* **2000**, *62*, 7809−7815.
(59) Valentine, A. J. S.; Li, X. Toward the Evaluation of Intersystem Crossing Rates with Variational Relativistic Methods. *J. Chem. Phys.* **2019**, *151*, 084107.
(60) Frisch, M. J.; Trucks, G. W.; Schlegel, H. B.; Scuseria, G. E.; Robb, M. A.; Cheeseman, J. R.; Scalmani, G.; Barone, V.; Petersson, G. A.; Nakatsuji, H.; Li, X.; Caricato, M.; Marenich, A. V.; Bloino, J.; Janesko, B. G.; Gomperts, R.; Mennucci, B.; Hratchian, H. P.; Ortiz, J. V.; Izmaylov, A. F.; Sonnenberg, J. L.; Williams-Young, D.; Ding, F.; Lipparini, F.; Egidi, F.; Goings, J.; Peng, B.; Petrone, A.; Henderson, T.; Ranasinghe, D.; Zakrzewski, V. G.; Gao, J.; Rega, N.; Zheng, G.; Liang, W.; Hada, M.; Ehara, M.; Toyota, K.; Fukuda, R.; Hasegawa, J.; Ishida, M.; Nakajima, T.; Honda, Y.; Kitao, O.; Nakai, H.; Vreven, T.; Throssell, K.; Montgomery, J. A., Jr.; Peralta, J. E.; Ogliaro, F.; Bearpark, M. J.; Heyd, J. J.; Brothers, E. N.; Kudin, K. N.; Staroverov, V. N.; Keith, T. A.; Kobayashi, R.; Normand, J.; Raghavachari, K.; Rendell, A. P.; Burant, J. C.; Iyengar, S. S.; Tomasi, J.; Cossi, M.; Millam, J. M.; Klene, M.; Adamo, C.; Cammi, R.; Ochterski, J. W.; Martin, R. L.; Morokuma, K.; Farkas, O.; Foresman, J. B.; Fox, D. J.*Gaussian Inc 16*, Revision A.03;Gaussian Inc.: Wallingford CT, 2016.
(61) Kasper, J. M.; Lestrange, P. J.; Stetina, T. F.; Li, X. Modeling $L_{2,3}$-Edge X-ray Absorption Spectroscopy with Real-Time Exact Two-Component Relativistic Time-Dependent Density Functional Theory. *J. Chem. Theory Comput.* **2018**, *14*, 1998−2006.
(62) Veryazov, V.; Widmark, P.-O.; Roos, B. O. Relativistic Atomic Natural Orbital Type Basis Sets for the Alkaline and Alkaline-Earth Atoms Applied to the Ground-State Potentials for the Corresponding Dimers. *Theor. Chem. Acc.* **2004**, *111*, 345−351.
(63) Roos, B. O.; Lindh, R.; Malmqvist, P.-A.; Veryazov, V.; Widmark, P.-O. Main Group Atoms and Dimers Studied with a New Relativistic ANO Basis Set. *J. Phys. Chem. A* **2004**, *108*, 2851−2858.
(64) Roos, B. O.; Lindh, R.; Malmqvist, P.-A.; Veryazov, V.; Widmark, P.-O. MNew Relativistic ANO Basis Sets for Transition Metal Atoms. *J. Phys. Chem. A* **2005**, *109*, 6575−6579.
(65) Roos, B. O.; Lindh, R.; Malmqvist, P.-A.; Veryazov, V.; Widmark, P.-O.; Borin, A. C. New Relativistic Atomic Natural Orbital Basis Sets for Lanthanide Atoms with Applications to the Ce Diatom and LuF3. *J. Phys. Chem. A* **2008**, *112*, 11431−11435.
(66) Pritchard, B. P.; Altarawy, D.; Didier, B.; Gibson, T. D.; Windus, T. L. New Basis Set Exchange: An Open, Up-to-Date Resource for the Molecular Sciences Community. *J. Chem. Inf. Model.* **2019**, *59*, 4814−4820.
(67) Adamo, C.; Barone, V. Toward Reliable Density Functional Methods Without Adjustable Parameters: The PBE0 Model. *J. Chem. Phys.* **1999**, *110*, 6158−6170.
(68) Becke, A. D. A New Mixing of Hartree−Fock and Local Density-Functional Theories. *J. Chem. Phys.* **1993**, *98*, 1372−1377.
(69) Huber, K. P.; Herzberg, G. H. In *NIST Chemistry WebBook, NIST Standard Reference Database Number 69*; Linstrom, P., Mallard, W., Eds.; National Institute of Standards and Technology: Gaithersburg, MD, p 20899, (retrieved January 15, 2022).
(70) LaJohn, L. A.; Ross, R. B.; Atashroo, T.; Ermler, W. C.; Christiansen, P. A. Ab Initio Relativistic Effective Potentials with Spin-Orblt Operators. III. Rb Through Xe. *J. Chem. Phys.* **1987**, *87*, 2812−2824.
(71) LaJohn, L. A.; Ross, R. B.; Powers, J. M.; Atashroo, T.; Ermler, W. C.; Christiansen, P. A. Ab Initio Relativistic Effective Potentials with Spin-Orbit Operators. IV. Cs Through Rn. *J. Chem. Phys.* **1990**, *93*, 6654−6670.
(72) Noro, T.; Sekiya, M.; Koga, T. Segmented Contracted Basis Sets for Atoms H Through Xe: Sapporo-(DK)-nZP Sets (n = D, T, Q). *Theor. Chem. Acc.* **2012**, *131*, 1124.
(73) Noro, T.; Sekiya, M.; Koga, T. Sapporo-(DKH3)-nZP (n = D, T, Q) Sets for the Sixth Period s-, d-, and p-Block Atoms. *Theor. Chem. Acc.* **2013**, *132*, 1363.
(74) Krishnan, R.; Binkley, J. S.; Seeger, R.; Pople, J. A. Self-Consistent Molecular Orbital Methods. XX. A Basis Set for Correlated Wave Functions. *J. Chem. Phys.* **1980**, *72*, 650−654.
(75) Francl, M. M.; Pietro, W. J.; Hehre, W. J.; Binkley, J. S.; Gordon, M. S.; DeFrees, D. J.; Pople, J. A. Self-Consistent Molecular Orbital Methods. XXIII. A Polarization-Type Basis Set for Second-Row Elements. *J. Chem. Phys.* **1982**, *77*, 3654−3665.
(76) McLean, A. D.; Chandler, G. S. Contracted Gaussian Basis Sets for Molecular Calculations. I. Second Row Atoms, Z = 11−18. *J. Chem. Phys.* **1980**, *72*, 5639−5648.
(77) Pacios, L. F.; Christiansen, P. A. Ab Initio Relativistic Effective Potentials with Spin-Orbit Operators. I. Li Through Ar. *J. Chem. Phys.* **1985**, *82*, 2664−2671.
(78) Hurley, M.; Pacios, L. F.; Ross, R. B.; Ermler, W. C.; Christiansen, P. A. Ab Initio Relativistic Effective Potentials with Spin-Orbit Operators. II. K Through Kr. *J. Chem. Phys.* **1986**, *84*, 6840−6853.
(79) Ross, R. B.; Gayen, S.; Ermler, W. C. Ab Initio Relativistic Effective Potentials with Spin-Orbit Operators. V. Ce Through Lu. *J. Chem. Phys.* **1994**, *100*, 8145−8155.
(80) Martins, L. S. C.; Jorge, F. E.; Machado, S. F. All-Electron Segmented Contraction Basis Sets of Triple Zeta Valence Quality for the Fifth-Row Elements. *Mol. Phys.* **2015**, *113*, 3578−3586.
(81) Gordon, M. S.; Binkley, J. S.; Pople, J. A.; Pietro, W. J.; Hehre, W. J. Self-Consistent Molecular-Orbital Methods. 22. Small Split-Valence Basis Sets for Second-Row Elements. *J. Am. Chem. Soc.* **1982**, *104*, 2797−2803.
(82) Ditchfield, R.; Hehre, W. J.; Pople, J. A. Self-Consistent Molecular-Orbital Methods. IX. An Extended Gaussian- Type Basis for Molecular-Orbital Studies of Organic Molecules. *J. Chem. Phys.* **1971**, *54*, 724−728.
(83) Devadas, M. S.; Bairu, S.; Qian, H.; Sinn, E.; Jin, R.; Ramakrishna, G. Temperature-Dependent Optical Absorption Properties of Monolayer-Protected Au25 and Au38 Clusters. *J. Phys. Chem. Lett.* **2011**, *2*, 2752−2758.
(84) Kang, X.; Chong, H.; Zhu, M. Hanbao Au25(SR)18: The Captain of the Great Nanocluster Ship. *Nanoscale* **2018**, *10*, 10758−10834.
(85) Cheshnovsky, O.; Brucat, P. J.; Yang, S.; Pettiette, C. L.; Craycraft, M. J.; Smalley, R. E. In *Physics and Chemistry of Small Clusters*; Jena, P., Ed.; Plenum Press: New York, 1987.
(86) Jiang, D.-e.; Kuhn, M.; Tang, Q.; Weigend, F. Superatomic Orbitals under Spin−Orbit Coupling. *J. Phys. Chem. Lett.* **2014**, *5*, 3286−3289.
(87) Altmann, S. L.; Herzig, P.*Point-Group Theory Tables*; Clarendon Press: Oxford, 2011.
(88) Petrone, A.; Williams-Young, D. B.; Sun, S.; Stetina, T. F.; Li, X. An Efficient Implementation of Two-Component Relativistic Density Functional Theory with Torque-Free Auxiliary Variables. *Euro. Phys. J. B* **2018**, *91*, 169.
(89) Liang, W.; Fischer, S. A.; Frisch, M. J.; Li, X. Energy-Specific Linear Response TDHF/TDDFT for Calculating High-Energy Excited States. *J. Chem. Theory Comput.* **2011**, *7*, 3540−3547.
(90) Lestrange, P. J.; Nguyen, P. D.; Li, X. Calibration of Energy-Specific TDDFT for Modeling K-Edge XAS Spectra of Light Elements. *J. Chem. Theory Comput.* **2015**, *11*, 2994−2999.
(91) Peng, B.; Lestrange, P. J.; Goings, J. J.; Caricato, M.; Li, X. Energy-Specific Equation-of-Motion Coupled-Cluster Methods for High-Energy Excited States: Application to K-Edge X-Ray Absorption Spectroscopy. *J. Chem. Theory Comput.* **2015**, *11*, 4146−4153.

https://doi.org/10.1021/jacsau.2c00659
JACS Au 2023, 3, 358−367